World Academy of Science, Engineering and Technology
International Journal of Mechanical and Mechatronics Engineering
Vol:15, No:8, 2021

Rolling Element Bearing Diagnosis by Improved Envelope Spectrum: Optimal Frequency Band Selection

Juan David Arango, Alejandro Restrepo-Martinez

***Abstract*—**The Rolling Element Bearing (REB) vibration diagnosis is worth of special interest by the variety of REB and the wide necessity of those elements in industrial applications. The presence of a localized fault in a REB gives rise to a vibrational response, characterized by the modulation of a carrier signal. Frequency content of carrier signal (Spectral Frequency –*f*) is mainly related to resonance frequencies of the REB. This carrier signal is modulated by another signal, governed by the periodicity of the fault impact (Cyclic Frequency –*α*). In this sense, REB fault vibration response gives rise to a second-order cyclostationary signal. Second order cyclostationary signals could be represented in a bi-spectral map, where Spectral Coherence –SCoh are plotted against *f* and *α*. The Improved Envelope Spectrum –IES, is a useful approach to execute REB fault diagnosis. IES could be applied by the integration of SCoh over a predefined bandwidth on the *f* axis. Approaches to select *f*-bandwidth have been recently exposed by the definition of a metric which intends to evaluate the magnitude of the IES at the fault characteristics frequencies. This metric is represented in a 1/3-binary tree as a function of the frequency bandwidth and centre. Based on this binary tree the optimal frequency band is selected. However, some advantages have been seen if the metric is changed, which in fact tends to dictate different optimal *f*-bandwidth and so improve the IES representation. This paper evaluates the behaviour of the IES from a different metric optimization. This metric is based on the sample correlation coefficient, detecting high peaks in the selected frequencies while penalizing high peaks in the neighbours of the selected frequencies. Prior results indicate an improvement on the signal-noise ratio (SNR) on around 86% of samples analysed, which belong to IMS database.

***Keywords*—**Sample Correlation IESFOgram, cyclostationary analysis, improved envelope spectrum, IES, rolling element bearing diagnosis, spectral coherence.

I. Introduction

THE REB vibration diagnosis is worth of special interest since the variety of REB, the diverse operational conditions in which are submitted, the wide necessity of those elements in industrial applications and the raise in reliability requirements are pursued by the nowadays-industrial context.

In a general point of view, the vibrational response of a bearing with a localized fault can be seen as a carrier signal with frequency content dictated by the resonance frequencies of the bearing and a modulation signal governed by the periodicity of the fault impact. In this sense, to explore the spectral content of the modulation signal i.e., explore the impact periodicity it results convenient to demodulate the signal from the carrier frequencies. In this process the high frequencies are intend to be separated by the low frequencies in order to read information in the range of frequencies at which the Fault Characteristics Frequencies (FCF) belong. To complete the demodulation, the amplitude envelope and the subsequent Envelope Spectrum (ES) analysis has been proved be extremely successful and has become the most useful approach in a variety of situations for the REB diagnosis [1].

ES could be obtained by cyclostationary analysis, as it is exposed in [2]. The cyclostationary analysis was applied to REB near two decades ago as [3] shown that an anomaly in a REB gives raise to a second order cyclostationary signal, which is mainly characterized by the fact the signals are non-stationary but hide a periodic behaviour in its variance. In this sense a REB localized fault vibration response signal can be represented in a bi-spectrum map, where the Spectral Correlation (SC) are plotted against Spectral Frequency – *f* and Cyclic Frequency – α. The earlier represents the dynamic characteristics of the REB i.e., their resonance frequencies whereas the second one represents the periodic behave of the fault [4]. SC are usually normalized to obtain the SCoh, in order to generate a blanket version improving the visualization and subsequently REB diagnosis process. In fact, [5] pointed out that the REB diagnosis by the cyclostationary analysis outperforms other classic methods such as the squared envelope spectral analysis by the use of Hilbert transform or even the Kurtogram benchmark method [6].

The REB diagnosis intents to track remarkable peaks at the REB characteristics frequencies [7] in the ES. In this intention the use of Enhanced Envelope Spectrum –EES or IES instead of ES achieves most desirable results. The EES is estimated by the integration of the SCoh over the entire *f*-axis, whereas IES is obtained in a similar way but integrating over a defined *f*-Bandwidth [8]. Recently focus has been put on the optimal way to select the *f*-Bandwidth, [9] proposed the IESFOgram use, which consists in a semi-exhaustive search optimization of a previously defined metric. This semi-exhaustive search is based on a 1/3 binary tree search. This approach of 1/3 binary three was originally proposed in the Fast Kurtogram [10], with the aim to determine the frequency band in which spectral kurtosis is maximized. The correct selection of the *f*-Bandwidth has been demonstrated to generate valuable aid for the diagnosis

Juan David Arango is with National University of Colombia, Colombia (e-mail: judarangoca@unal.edu.co).

over high impulsive non-Gaussian noise, which has been reported as challenging point in the state of the art [5], [9], [11]. In this paper, a modification on the IESFOgram is proposed. This modification is based on the use of the Sample Correlation Coefficient (SCC) between the IES and a desired spectrum. The use of this approach is compared with the EES and IES generated by original IESFOgram, namely IESFO, among the IMS data set [12]. Prior results indicate a favourable SNR with the use of SCC.

II. Signal Processing Methods for REB Diagnosis

Different authors have characterized the vibrational responses associated with a bearing fault. In general, a REB fault is seen as the response of a series of impacts generated by the contact between the surfaces of the REB and the surface in which the fault is located [13]. The periodicity of those impacts is dictated by the REB's kinematics characteristics, i.e., the rotation velocity and the REB geometry, as indicated by the well-known FCF (BPFI, BPFO, BSF, FTF) [7]. Those impacts stimulate the resonance frequencies of the REB, which in fact, lie on the range of 2-10 kHz, those frequencies are dictated by the dynamic characteristics of the REB, i.e., mass, lumped and stiffness. On the other hand, the FCF usually do not overcome 1 kHz. In this sense, a duality in the REB vibration response is seen. This duality generates a vibration signal in which the high frequencies (related with dynamic features of REB) are modulated by the FCF (low frequencies).

The major part of signal processing tools for REB diagnosis tends to demodulate the signal in order to visualize the spectral content of the modulation frequencies and compare them with the FCF.

A. Spectral Correlation

As previously mentioned, a localized fault in a REB gives rise to a series of periodic impulses. These impulses are not strictly periodic, since the slippage of the rolling element generates a random behaviour on the time arrival of those impulses. This random component generates a second order cyclostationary vibration response. This in fact is true for REB under large spall faults [14]. Second order cyclostationary signals are characterized by having a periodic autocorrelation function R_{xx} [15]. The autocorrelation function is expressed as indicated in (1):

$$R_{xx}(t,\tau) = E[x(t)x^*(t-\tau)] \tag{1}$$

In (1) t, τ stands for the time and time lag respectively; $E[\cdot]$ represents the expected value operator, and the * superscript denotes the complex conjugate.

SC is a valuable tool for representing the information contained in the autocorrelation function in frequency terms. The SC is a bi-dimensional function, which depends on the spectral frequency *(f)* and the cyclic frequency *(α)* as it is described in (2) [16]:

$$S_{xx}(\alpha,f) = E\left[X\left(f-\frac{\alpha}{2}\right)X^*\left(f+\frac{\alpha}{2}\right)\right] \tag{2}$$

where $X(f)$ is the Fourier transform of the signal *x*.

SC measures the correlation between at two frequencies which are separated at α. If a high correlation is achieved, it means that the spectral frequency *f* is strongly modulated at cyclic frequency α. In this sense, SC allows to determine modulations in the vibration response signal. Particularly in a localized fault in a REB, the cyclic frequency in the SC describes the periodic behaviour related with the impact time arrival whereas the spectral frequency f represents the frequencies which are excited by the impact i.e., the carrier frequency.

According to the previous discussion, when a REB presents a localized fault, high SC should be identified where the cyclic frequency equals the FCF and/or their harmonics.

For exploring the SC among the cyclic frequencies, a one-dimensional spectrum could be obtained from the SC bi-map. This is done by integrating the SC over the *f-axis* as indicated by (3):

$$ES(\alpha) = \frac{1}{Fs}\int_0^{Fs/2} |S_{xx}(\alpha,f)|df \tag{3}$$

where ES stands for the Envelope Spectrum and *Fs* represents the sampling frequency. It is important to note that the ES obtained by (3) stands for the same ES obtained by the use of Hilbert transform. It has been demonstrated by [2].

As a manner of whitening the vibration response signal, the SCoh is usually preferred over the SC. SCoh is exposed in (4):

$$\gamma_{xx}(\alpha,f) = \frac{S_{xx}}{\sqrt{S_{xx}(0,f)\cdot S_{xx}(0,f+\alpha)}} \tag{4}$$

In a similar way, one-dimensional spectrogram from the SCOh could be obtained by integrating over the *f* axis. When the integration is done over the entire *f* axis it is called EES as it is shown in (5):

$$EES(\alpha) = \frac{1}{Fs/2}\int_0^{Fs/2} \gamma(\alpha,f)df \tag{5}$$

When a selected interval of the *f* axis is selected to perform the integration, it is called IES as it is shown in (6):

$$IES(\alpha;f_c,\Delta f) = \frac{1}{\Delta f}\int_{f_c-\Delta f/2}^{f_c+\Delta f/2} \gamma(\alpha,f)df \tag{6}$$

where f_c and Δf represent the center frequency and the bandwidth of the selected spectral frequency interval, respectively.

B. Kurtogram

As described earlier, a localized fault in a REB generates a series of periodical impacts. Those periodical impacts usually stimulate the resonance frequencies of the REB or even the resonance frequency of the vibration sensor coupling. In this sense, a strategy to demodulate the signal is try to find the range of frequencies in which the natural frequencies belong, and so filter the signal on this particular range. Once the signal is filtered, the ES could be analysed in order to compare if there

is evidence on noticeable peaks at the FCF.

The impacts generated by the REB faults usually generate high kurtosis signals, and based on this idea, the frequency bandwidth of the signal should be selected trying to maximize the Spectral Kurtosis. Spectral kurtosis on its definition suffers of taking long computational expense and strong dependence on the parameters selected for this computation. To deal with this, the Kurtogram has been proposed [10]. In this tool, the signal is filtered over a series of bandwidths, in a manner of 1/3-binary tree and the sample kurtosis is computed for each of the filtered signal. The 1/3 binary tree Kurtogram is kind of heat map where the kurtosis function is evaluated at different centre frequencies and bandwidths. It is illustrated in Fig. 1. By the Kurtogram use, the filter band is selected by taking f_c and Δf which enhance the maximum value of kurtosis. From this filtered signal, the square envelope is computed and consequently analysed.

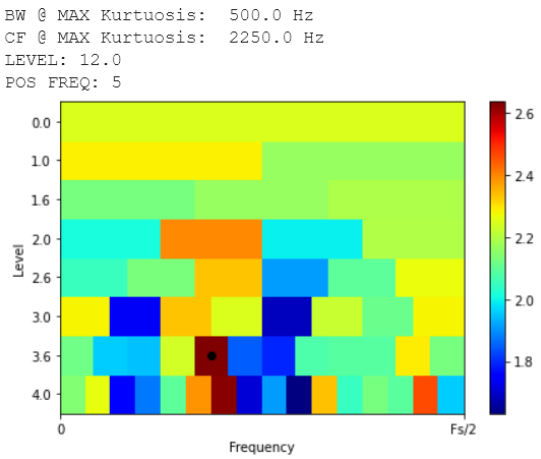

Fig. 1 Kurtogram 1/3 binary tree illustration

The idea of a semi-exhaustive search based on the 1/3-binary tree representation could be extended to another kind of variable optimization. This idea would be used for the rest of the paper.

C. IESFOgram

As it is mentioned, usually it is common to try to represent the cyclic frequencies on a one-dimensional spectrogram. In fact, the IES has been proved to represent a valuable tool for REB fault diagnosis. The use of IES in place of EES stands by the fact that commonly the FCF do not modulate all the spectral content, but modulate selected frequency ranges. The latter indicates that an adequate selection of f_c and Δf for the IES determination could improve notoriously the one-dimensional spectrum representation, and so on the diagnosis process.

Recently, [9] has proposed a method for the semi-automatic selection of the optimal frequency band for the IES computation. The resulting IES is namely IESFO standing for IES Frequency Optimization. This method was applied to REB diagnosis under high impulsive noise coming for Pulse-Width Modulation (PWM). In this approach, a metric is represented as a function of the spectral frequency band. The metric selected in this proposed method corresponds to the sum of the IES evaluated over a set of cyclic frequencies previously selected, as it shown in (7):

$$Ind = \sum_k IES(\alpha_k; f_c, \Delta f) \tag{7}$$

where α_k could represent the k^{TH} candidate of cyclic frequency in which a track of fault should appear. It is important to mention that probably the set of cyclic frequencies correspond to the harmonics of the FCF prior selected. In this sense, optimal frequency band is done by representing the *Ind*-metric in a 1/3-binary tree, in a similar manner as Kurtogram is presented. The optimal spectral frequency band is then selected by maximum value observing in which centre frequency and frequency bandwidth the *Ind*-metric reaches the maximum. This approach has been named IESFOgram.

III. Proposed Method

A. Ind-Metric Discussion

To further explore IES computation from the use of IESFOgram and the *Ind* computation let us analyse Fig. 2. A set of three cyclic frequencies are prior selected $\{\alpha_1, \alpha_2, \alpha_3\}$. Additionally, let's suppose that a spectral frequency band (f_1 and f_2) is also prior selected by the use of IESFOgram. From the SCoh (Fig. 2 (a)) the IES is computed by the integration between f_1 and f_2 over the *f-axis* as it is illustrated in (6). The IES is then evaluated at the set of cyclic frequencies, and the magnitudes obtained are added to compute the *Ind* metric as it is shown in (7), this process is schematized in Fig. 2 (b)

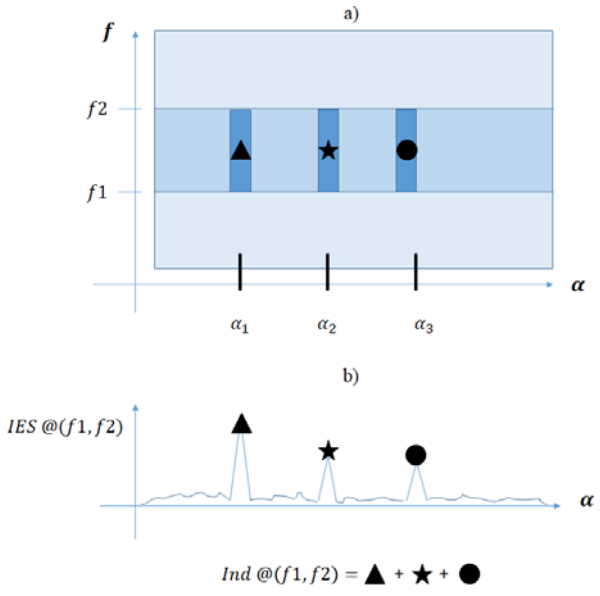

Fig. 2 Illustration of IES and Ind-metric computation

For REB diagnosis, it is desirable to obtain a spectrogram where the magnitude of the IES looks as close as possible to delta functions in the FCF. It means the desired shape of the IES reaches high magnitude value in those FCF whereas the neighbour magnitudes keep close to zero. From the last idea, it results important to explore the nature of the metric used in the

IESFOgram. Although the metric intends to maximize the amplitude on the selected FCF, it does not evaluate the IES on the neighbour cyclic frequencies. This is illustrated in Fig. 3 where two IES generate the same Ind despite of their noticeable differences on their behaviour. In Fig. 3 (a) the IES do not keep zero at the neighbour of the selected FCF, whereas the IES shown in Fig. 3 (b) does.

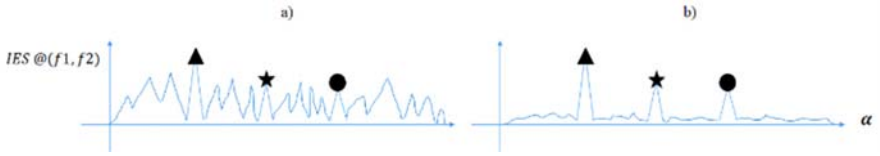

Fig. 3 Ind-metric computation comparison

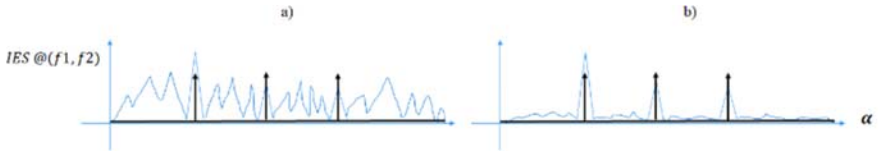

Fig. 4 Sample correlation computation comparison

In order to generate a different metric, which evaluates a high peak in the selected FCF, but at the same time evaluates the neighbour behave, the SCC between the IES and a hypothetic IES is proposed. The hypothetic IES results equivalent to the sum of delta functions on the FCF and their harmonics. This idea is illustrated in Fig. 4 and described by (8) in their discrete form. In Fig. 4 (a), an IES has small sample correlation with respect to the hypothetic IES, this is because the magnitude of IES on FCF's neighbour cyclic frequencies is considerable. In contrast, Fig. 4 (b) has big sample correlation because of their similitude with the desire delta function.

Sample correlation is high when

$$r = \frac{\sum_k (IES[k]-\overline{IES})(IES_{desired}[k]-\overline{IES}_{desired})}{\sqrt{\sum_k (IES[k]-\overline{IES})^2 (IES_{desired}[k]-\overline{IES}_{desired})^2}} \quad (8)$$

where the ¯ stands for the mean operator.

The optimal spectral frequency band could also be obtained by the 1/3-binary tree search in a similar way than an IESFOgram or a Kurtogram. With the only aim of simplicity, this approach is named newIESFOgram. The resulting IES generated is named newIESFO in analogous manner.

IV. Methods and Procedures

A. IMS Database

IMS database is a valuable database, which contains run to failure experimentation of REB [12], [17]. The database contains three experimental runs, each one contained in a separate database. The test rig is shown in Fig. 5 [12], [18]. It consists of an electric motor, coupled to a shaft by a belt. The shaft is supported on four bearings. A radial load is applied to the shaft by charging it on the bearings 2 and 3.

During the second and third experimental runs, the test rig was operated continuously until fault evidences on the bearing 1-outer race, and bearing 2-outer race were reached respectively. During first experimental run the rigs were operated by intervals until evidences of faults on bearing 3-inner race and bearing 4-rolling element were identified.

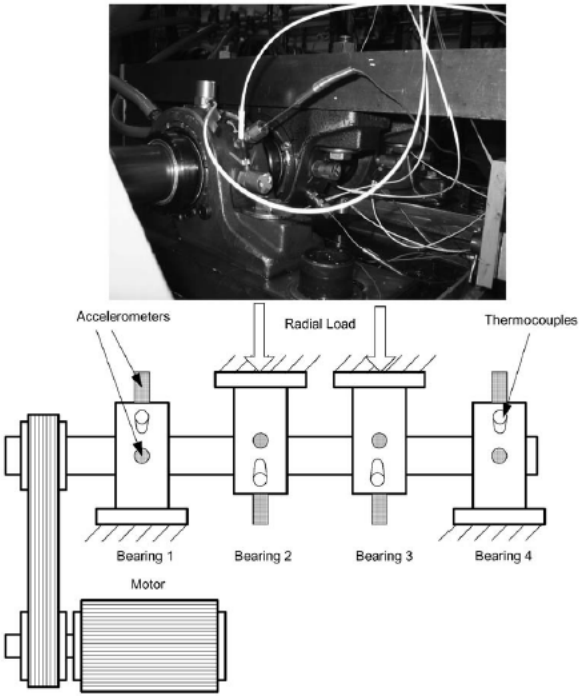

Fig. 5 IMS test rig scheme, taken from [17]

In each run, records were taken each 10 minutes, where each record contains 8 channels sampled at 20 kHz (although for the authors perception it was sampled with a rate of 20.48 kHz). Only in the first run all channels were filled with accelerometer signals, corresponding to accelerometers installed in each one of the four REB at the horizontal and vertical positions. In second and third experimental run, vibrations were only measured at one position. FCF are shown in Table I. Detailed description on this dataset could be obtained at the "readme" file attached to the downloaded file [17].

TABLE I
FCF FOR REB ON THE IMS DATASET

Characteristic Frequency	Numerical Value [Hz]
Shaft rotation frequency (RPS)	33.3
Ball Pass Frequency Outer Race (BPFO)	236
Ball Pass Frequency Inner Race (BPFI)	297
Ball Spin Frequency (BSF)	278
Fundamental Train Frequency (FTF)	15

Example of a vibration signal available in IMS data set and RMS evolution for the second experimental run is shown in Fig. 6. The entire 2nd experimental run was processed computing the Root Mean Square (RMS) for the entire 988 records in each of the four bearings sensors, this is shown in Fig. 7. It could be observed that RMS measured on the bearing 1 increases as time increases due to the bearing fault degradation (fault on the outer race). The same behaviour is observed on the rest of bearings but in lesser degree. The latter is because the vibration generated on bearing 1 is lumped through the shaft, and so, results less evident on the other sensors.

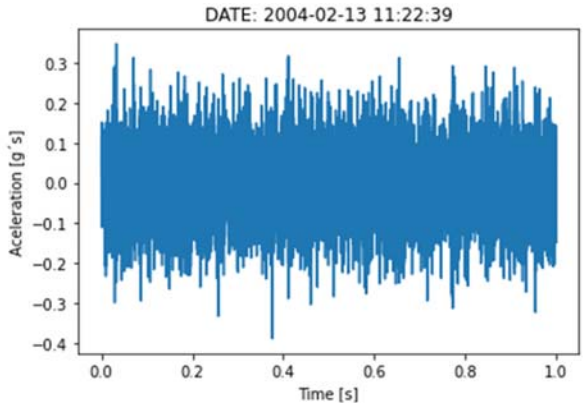

Fig. 6 Time waveform File '2004.02.13.11.22' – Bearing 1 (Record number 150)

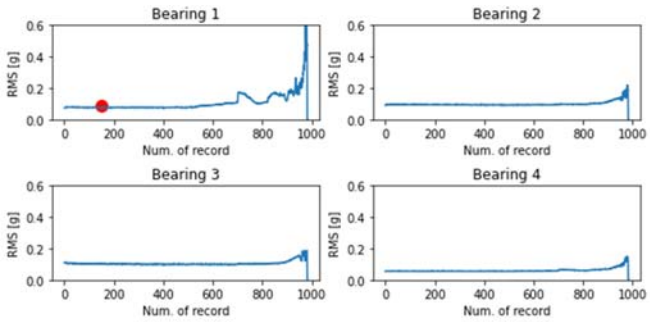

Fig. 7 RMS time-history for measurement in the 2nd run data-set

B. newIESFOgram Method

To illustrate the use of IESFOgram and the modification proposed in this paper, let us analyse a signal taken on the Bearing 1 during the second run, this signal is extracted from file labelled '2004.02.13.11', this file corresponds to the record number 150 and their time-waveform was previously shown in Fig. 6. The RMS of this signal has been marked by a red dot on Fig. 7.

SC estimated by the Antoni fast SC algorithm is shown in Fig. 8 [19]. From this figure a vertical contrast can be seen near to cyclic frequency 236 Hz, which tends to coincide with the BPFO as it was expected, by the report on the IM documentation. This vertical contrast is even more clear in the spectral frequency range between 6 kHz and 10 kHz as it is remarked by the red rectangle drawn in Fig. 8.

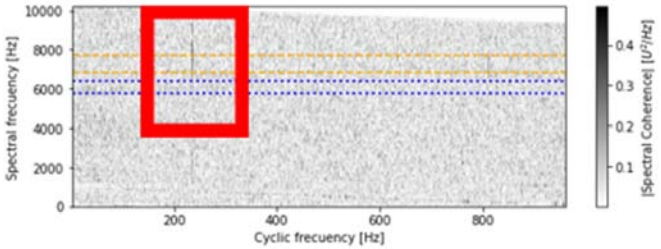

Fig. 8 *SCoh* for the '2004.02.13.11.22' file (Record number 150)

Considering the first three harmonics of the BPFO as the selected cyclic frequencies, the INFOgram is plotted in Fig. 9. In a similar manner the INFOgram based on sample correlation is shown in Fig. 10. Based on the INFOgram the optimal spectral frequency lies in the range of 5.44 kHz and 6.72 kHz, which are marked by the dot on drawn on Fig. 9. On the other hand, by the use of the newIESFOgram the optimal spectral frequency range is the range between 6.4 kHz and 8.11 kHz. We notice the differences between the optimal levels selected i.e., the frequency bandwidth and the centre frequency location. In this particular case, the newIESFOgram dictates that the optimal frequency band lies on bigger frequencies and is less selective than the frequency band dictated by the IESFOgram.

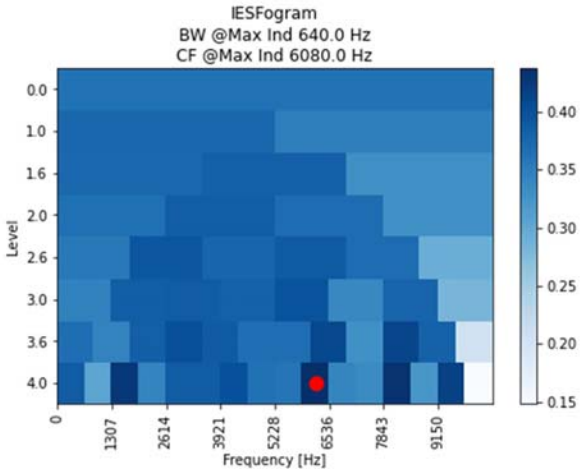

Fig. 9 IESFOgram for '2004.02.13.11' Bearing 1 signal. Optimal frequency band selected [5.76 kHz; 6.40 kHz]

The previous discussion is further illustrated by the horizontal lines plotted in Fig. 8, where the blue-dotted line represents the frequency band dictated by the IESFOgram and the orange dashed line represents the frequency band dictated by the newIESFOgram (the colours for those lines are analogous to colour map in Figs. 9 and 10). We notice that the

SCoh reaches higher magnitude value in the frequency range closed by orange-dashed lines (i.e., newIESFOgram). In contrast, at the frequency range dictated by blue-dashed lines (i.e., IESFOgram) it is not possible to identify any vertical contrast.

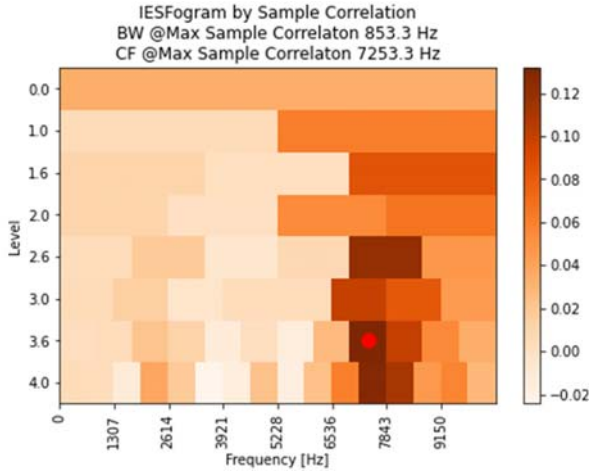

Fig. 10 newIESFOgram for '2004.02.13.11' Bearing 1 signal. . Optimal frequency band selected [6.83 kHz; 7.68 kHz]

Comparison of EES, IESFO and newIESFO are shown in Fig. 11. In the EES, a noticeable peak at the BPFO is easily identified, however this peak is not identifiable by the IESFO. In contrast, newIESFO results the clearest spectral one-dimensional. The previous discussion indicates that newIESFO facilitates the REB diagnosis.

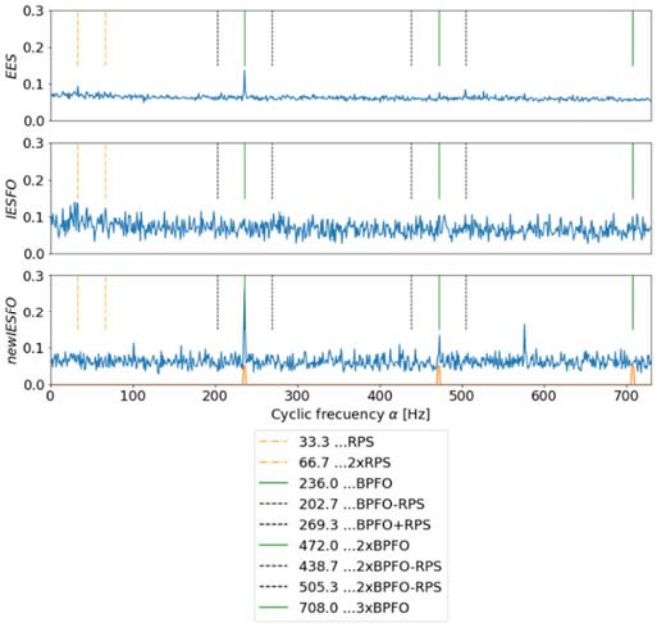

Fig. 11 EES, IESFO and newIESFO comparison for Bearing 1 in '2004.02.13.11' record number 150 of 2nd dataset.

C. Metric Comparison

As it has been discussed, the IESFOgram and newIESFOgram dictate the optimal frequency band in which the SCoh should be integrated in order to facilitate the bearing fault diagnosis by the analysis of the IES. In this sense there is a necessity of a measurement for the degree in which fault can be diagnosed on the IES. For this purpose, an SNR estimator is proposed and expressed in (9):

$$\widehat{SNR} = \frac{\sum_k IES(\alpha_k; f_c, \Delta f)^2}{\|IES(\alpha)\|^2} \quad (9)$$

where α_k represents the pre-defined cyclic frequencies to analyse. This estimator valuates high peaks on the pre-defined cyclic frequencies in relation with the magnitude of the entire IES vector.

V. Results

A. Analysis of the Entire 2nd Run IMS Dataset

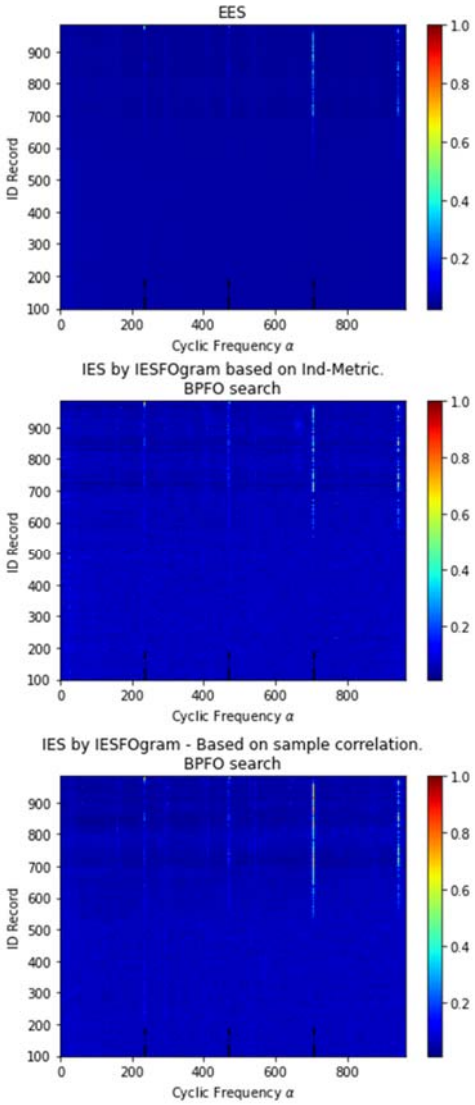

Fig. 12 EES and IESFO and newIESFO along 2nd IM experimental run

In this section, the results of applying the newIESFO approach are compared with the IESFO approach among the

entire 2nd run data set. Additionally, a particular analysis is carried out with the aim of evaluating the proposed approach in terms of earlier detection capacity. The section finalizes with the analysis of a case where the SNR estimator favours the IESFO method.

The analysis of the IES obtained using IESFOgram and newIESFOgram has been done over the entire 2nd IMS run data set. This is shown in Fig. 12, where the EES, IESFO and newIESFO are plotted against the record numbers (vertical axes). The black-dashed cursors drawn in Fig. 12 are set at the first three harmonics of BPFO. More marked contrast is generally achieved in the new-IESFO, particularly when we consider the third harmonic of BPFO ($\alpha \approx 708$ Hz).

Now let's analyse the behaviour of the SNR estimator for the IESFO and newIESFOgram among the entire 2nd run dataset as plotted in Fig. 13. Based on the SNR estimator, the newIESFO tends to outperform the IESFOgram, since the orange line is almost always above the blue line. The marked increase in the value of SNR around record number 550 is explained by the more noticeable mark of the bearing 1 outer race fault. The decay on the SNR estimator decay observed on samples between the 700TH and 780TH could be generated by the growing of the outer race fault which could augment the overall vibration and so reducing the SNR because of their relativeness.

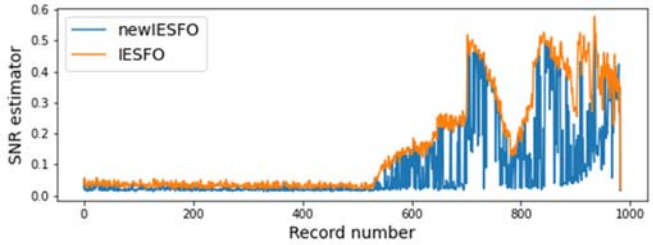

Fig. 13 SNR estimator comparison among the entire 2nd experimental run

The general improvements on the SNR by the use of newIESFO could also be observed in the boxplot shown in Fig. 14, where the blue boxplot represents the SNR for the newIESFO among the entire 2nd run dataset, and the orange boxplot represents the proper but at the IESFO. It is possible to visualize that orange boxplot is generally located in an upper position, indicating there is more cases where $SNR_{newIESFOgram} > SNR_{IESFOgram}$ as indicated in Table II.

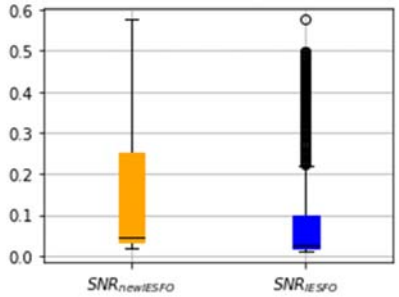

Fig. 14 Boxplot for SNR estimator on IESFO and newIESFO among 2nd run data set

TABLE II
SNR ESTIMATOR AMONG ENTIRE 2ND IMS DATASET (BEARING SIGNALS): APPROACHES COMPARISON

SNR Estimator Comparison	Amount of Samples
newIESFO bigger SNR than IESFO	860 (87%)
newIESFO lesser SNR than IESFO	39 (4%)
newIESFO equal SNR than IESFO	85 (9%)

B. Comparison by Earlier Diagnosis Ability

Generating earlier diagnosis in REB is one of the most relevant features pursued by the different diagnosis approaches. To illustrate this, let's analyse the use of the INFOgram and newINFOgram in face to the earlier diagnosis capacity. For the author's analysis in the 2nd IMS data set, signatures of outer race fault on bearing 1 were observed since their first record ('2004.02.12.10.32.39'), although their RMS value results relatively small as it was observed in Fig. 7. This record is then considered as a candidate signal to be analysed for the aim of evaluate the earlier detection capacity of the IESFO and newIESFO. The '2004.02.12.10.32.39' record time wave-form is shown in Fig. 15.

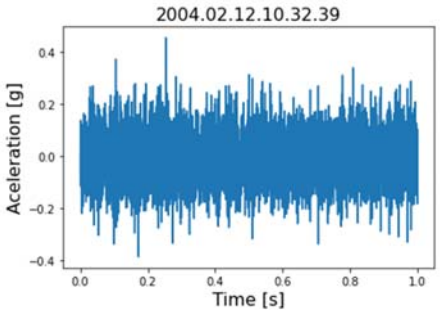

Fig. 15 Time waveform of the first record on the 2nd IMS run sampled on bearing 1

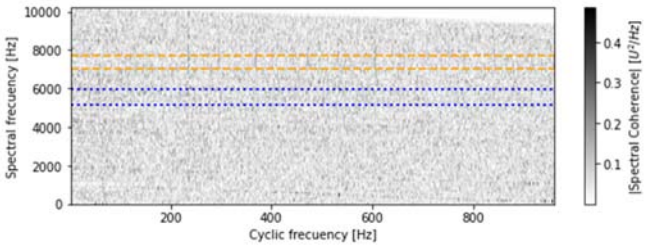

Fig. 16 *SCoh* for first record on the 2nd IMS run.

The SCoh and the newIESFOgram are shown in Figs. 16 and 17. The orange-dashed lines and the blue-dotted lines on Fig. 16 correspond to the spectral frequency bands dictated by the IESFOgram and newIESFOgram respectively. Notice that the highest vertical contrast of the SCoh belongs to the band dictated by newIESFOgram.

The IESFO and newIESFO are plotted in Fig. 18. While the INFOgram dictates the spectral frequency band between 5973.3 and 6826.6 Hz as the optimal frequency band, the newIESFOgram dictates that the 8960.0 and 9600.0 kHz corresponds to the optimal frequency band.

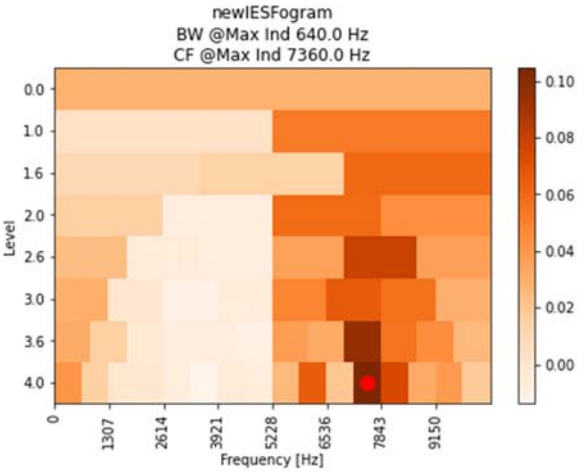

Fig. 17 newIESFOgram for first record on the 2nd IMS run

The SNR estimator takes values of 0.022 and 0.037 for the IESFO and newIESFO respectively. According to this SNR comparison, the newIESFO allows to compute a better representation for the IES when the signal feature is weak.

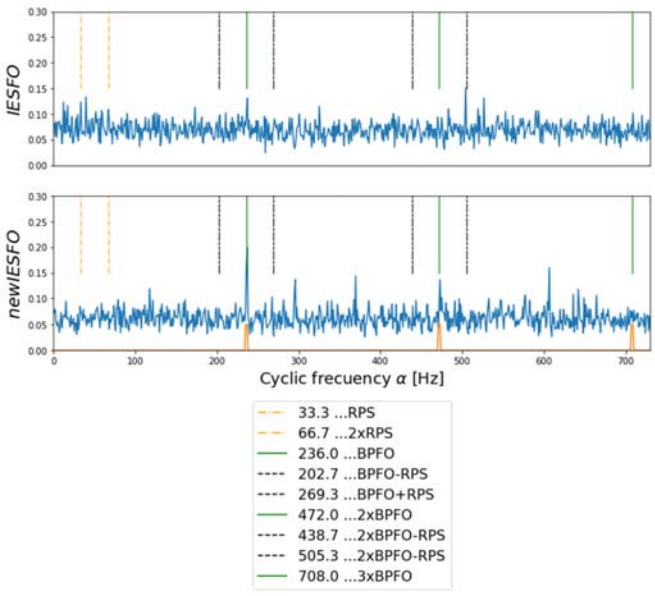

Fig. 18 IESFO and newIESFO for first record on the 2nd IMS run Bearing 1 signal

C. Comparison for IESFO Outperforming newIESFO

It results interesting to pay attention in those signals were the IESFO outperforms the newIESFO (based on SNR estimator). In particular, among the 2nd IMS dataset, the record number 980 (Corresponding to file '2004.02.18.15.02.39') contains the signal where the difference $SNR_{IESFO} - SNR_{newIESFO}$ takes a maximum value. The record number 980 signal time waveform is shown in Fig. 20.

In analogous manner to the previous analysis, the SCoh and the newIESFOgram are shown in Figs. 21 and 22. The blue-dotted lines on Fig. 21 represent the frequency band dictated by IESFOgram whereas orange-dashed lines represent the frequency band dictated by newIESFOgram. Although both approaches dictate spectral bands considerably separated, the vertical contrast at BPFO (~236 Hz) does not show marked differences. This in fact is illustrated in Fig. 23, where the IESFO and newIESFO are plotted. Notice that in both spectra the failure at BPFO is evident by the presence of remarkable peaks at the BPFO and their two first harmonics. For this particular case, it is possible to conclude that although the SNR estimator favours the IESFO, the newIESFO results are satisfactory.

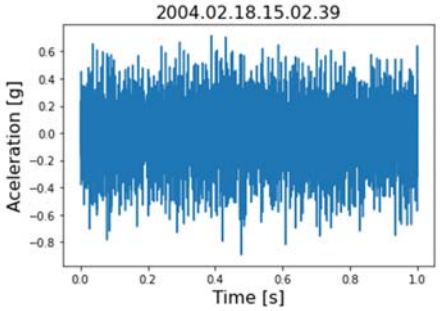

Fig. 20 Time waveform of the record 980 of the 2nd IMS run sampled on bearing 1

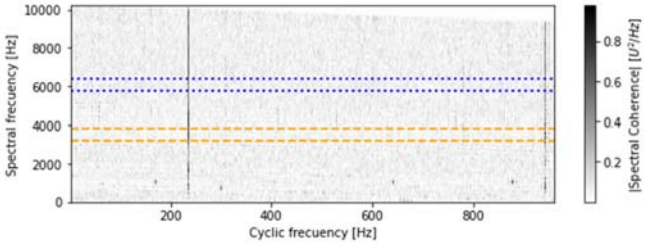

Fig. 21 SCoh for record number 980 of the 2nd IMS run

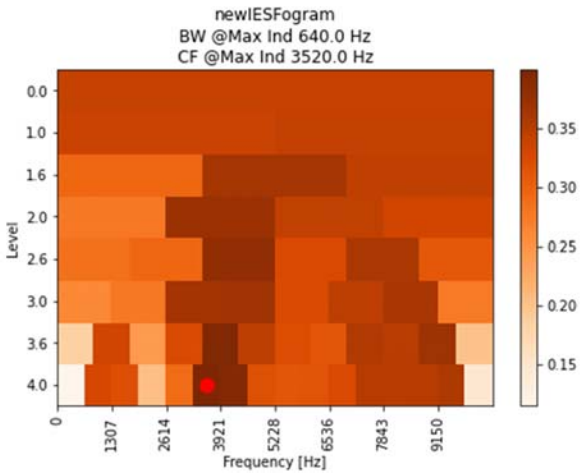

Fig. 22 newIESFOgram for record number 980 on the 2nd IMS run

As it can be seen, although there is a better performance for the IESFO by the use of newIESFO an adequate diagnosis could be done. In fact, in this case the spectral frequency bands dictated by each one are considerably similar, in the first case the frequency band corresponds to the interval [2560.0; 3200.0]

kHz, whereas the second one corresponds to the interval [1920.0; 2560.0] kHz, which are illustrated on the SCoh bi-map (Fig. 18). The strong vertical contrast presented in the SCoh at the BPFO gives certain degree of freedom to the algorithms discussed.

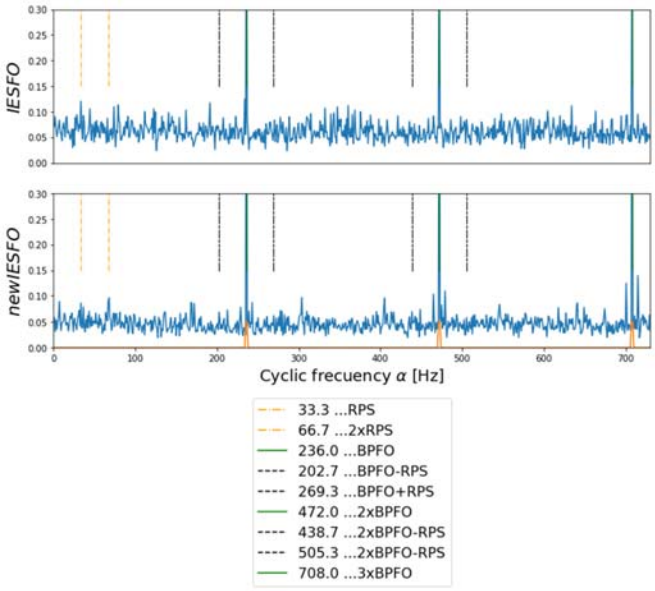

Fig. 23 IESFO and newIESFO for first record on the 2nd IMS run Bearing 1 signal

VI. Conclusion

The REB fault diagnosis has been studied in an intensive way since last two decades. For this purpose, the SCoh represents an invaluable tool. From SCoh, the EES and IES could be obtained. The IES requires the selection of particular spectral frequencies ranges, to premediate the SCoh along *f-axis.* The IESFOgram is an interesting tool for selecting the optimal frequency band (*fc* and *Δf*). In this sense, the *Ind* metric (which is the sum of the IES evaluated in a set of selected cyclic frequencies) is expressed as a function of the frequency band in a 1/3-binary tree, which allows to visualize what is the optimum frequency band. In the same sense, the newIESFOgram utilizes the same principle but the metric is changed by the sampling correlation between the IES and a hypothetical IES composed by delta functions at the selected cyclic frequencies. This is proposed with the intention to do not favour uniquely the high peaks at $\{\alpha_k\}$, but the neighbour behaviour. By utilizing both approaches on the IMS data-set, clearer IES are obtained. However, by comparing the two approaches some advantages are observed by the use of the newIESFOgram. If an SNR estimator is used as an evaluation metric, over the entire 2nd run IMS Data-set of the cases the SNR for the IESFO is greater than the newIESFO. The SNR of the newIESFO is greater than SNR of the IESFO in 87% of the cases.

By comparing the IESFO and newIESFO in face to the earlier detection, advantages are also observed and discussed. From the authors point of view, this simple modification on IESFO could lead to interesting improvements in REB diagnosis.

References

[1] R. B. Randall and J. Antoni, "Rolling element bearing diagnostics---A tutorial," *Mech. Syst. Signal Process.*, vol. 25, no. 2, pp. 485–520, 2011.

[2] R. B. Randall, J. Antoni, and S. Chobsaard, "The relationship between spectral correlation and envelope analysis in the diagnostics of bearing faults and other cyclostationary machine signals," *Mech. Syst. Signal Process.*, vol. 15, no. 5, pp. 945–962, 2001.

[3] A. C. McCormick and A. K. Nandi, "Cyclostationarity in Rotating Machine Vibrations 1 Introduction 2 Wide-sense Cyclostationarity," *Mech. Syst. Signal Process.*, vol. 12, no. 2, pp. 225–242, 1998.

[4] J. Antoni, F. Bonnardot, A. Raad, and M. El Badaoui, "Cyclostationary modelling of rotating machine vibration signals," *Mech. Syst. Signal Process.*, vol. 18, no. 6, pp. 1285–1314, 2004.

[5] D. Abboud, M. Elbadaoui, W. A. Smith, and R. B. Randall, "Advanced bearing diagnostics: A comparative study of two powerful approaches," *Mechanical Systems and Signal Processing*, vol. 114. pp. 604–627, 2019.

[6] W. A. Smith and R. B. Randall, "Rolling element bearing diagnostics using the Case Western Reserve University data: A benchmark study," *Mech. Syst. Signal Process.*, vol. 64–65, pp. 100–131, 2015.

[7] I. Howard, "A Review of Rolling Element Bearing Vibration 'Detection, Diagnosis and Prognosis,'" *DSTO-AMRL Report, DSTO-RR-00113*, no. October 1994, pp. 35–41, 1994.

[8] D. Wang, X. Zhao, L. L. Kou, Y. Qin, Y. Zhao, and K. L. Tsui, "A simple and fast guideline for generating enhanced/squared envelope spectra from spectral coherence for bearing fault diagnosis," *Mech. Syst. Signal Process.*, vol. 122, no. January, pp. 754–768, 2019.

[9] A. Mauricio *et al.*, "Bearing diagnostics under strong electromagnetic interference based on Integrated Spectral Coherence," *Mech. Syst. Signal Process.*, vol. 140, p. 106673, 2020.

[10] J. Antoni, "Fast computation of the kurtogram for the detection of transient faults," *Mech. Syst. Signal Process.*, vol. 21, no. 1, pp. 108–124, 2007.

[11] P. Borghesani and J. Antoni, "CS2 analysis in presence of non-Gaussian background noise – Effect on traditional estimators and resilience of log-envelope indicators," *Mech. Syst. Signal Process.*, vol. 90, pp. 378–398, 2017.

[12] J. Lee, H. Qiu, G. Yu, J. Lin, and Rexnord Technical Services, "'Bearing Data Set', NASA Ames Prognostics Data Repository." IMS, University of Cincinnati, 2007.

[13] P. D. McFadden and J. D. Smith, "Vibration monitoring of rolling element bearings by the high-frequency resonance technique --- a review," *Tribology International*, vol. 17, no. 1. pp. 3–10, 1984.

[14] J. Antoni, "Cyclic spectral analysis of rolling-element bearing signals: Facts and fictions," *J. Sound Vib.*, vol. 304, no. 3–5, pp. 497–529, 2007.

[15] J. Antoni, "Cyclostationarity by examples," *Mech. Syst. Signal Process.*, vol. 23, no. 4, pp. 987–1036, May 2009.

[16] J. Antoni, "Cyclic spectral analysis in practice," *Mech. Syst. Signal Process.*, vol. 21, no. 2, pp. 597–630, 2007.

[17] H. Qiu, J. Lee, J. Lin, and G. Yu, "Wavelet filter-based weak signature detection method and its application on rolling element bearing prognostics," *J. Sound Vib.*, vol. 289, no. 4–5, pp. 1066–1090, 2006.

[18] W. Gousseau, J. Antoni, F. Girardin, and J. Griffaton, "Analysis of the rolling element bearing data set of the center for intelligent maintenance systems of the University of Cincinnati," *13th Int. Conf. Cond. Monit. Mach. Fail. Prev. Technol. C. 2016/MFPT 2016*, 2016.

[19] J. Antoni, G. Xin, and N. Hamzaoui, "Fast computation of the spectral correlation," *Mech. Syst. Signal Process.*, vol. 92, pp. 248–277, 2017.